Crystal structure of chlorite dismutase, a detoxifying enzyme producing molecular oxygen

Geus, D.C. de; Hagedoorn, P.L.; Pannu, N.S.; Duijn, E. van; Abrahams, J.P.; Thomassen, E.A.J.

doi:10.1016/j.jmb.2009.01.036 J. Mol. Biol. (2009) 387, 192–206

JMB

Available online at www.sciencedirect.com

ScienceDirect

ELSEVIER

Crystal Structure of Chlorite Dismutase, a Detoxifying Enzyme Producing Molecular Oxygen

Daniël C. de Geus[1]*, Ellen A. J. Thomassen[1], Peter-Leon Hagedoorn[2], Navraj S. Pannu[1], Esther van Duijn[3,4] and Jan Pieter Abrahams[1]

[1]*Department of Biophysical Structural Chemistry, Leiden Institute of Chemistry, Leiden University, Einsteinweg 55, 2333 CC Leiden, The Netherlands*

[2]*Department of Biotechnology, Delft University of Technology, Julianalaan 67, 2628 BC Delft, The Netherlands*

[3]*Biomolecular Mass Spectrometry and Proteomics Group, Bijvoet Center for Biomolecular Research and Utrecht Institute for Pharmaceutical Sciences, Utrecht University, Sorbonnelaan 16, 3584 CA Utrecht, The Netherlands*

[4]*Netherlands Proteomics Center, Sorbonnelaan 16, 3584 CA Utrecht, The Netherlands*

Received 9 September 2008; received in revised form 16 January 2009; accepted 20 January 2009
Available online 27 January 2009

Edited by R. Huber

Chlorite dismutase (Cld) is a key enzyme of perchlorate and chlorate respiration. This heme-based protein reduces the toxic compound chlorite into the innocuous chloride anion in a very efficient way while producing molecular oxygen. A sequence comparison between Cld homologues shows a highly conserved family. The crystal structure of *Azospira oryzae* strain GR-1 Cld is reported to 2.1 Å resolution. The structure reveals a hexameric organization of the Cld, while each monomer exhibits a ferredoxin-like fold. The six subunits are organized in a ring structure with a maximal diameter of 9 nm and an inner diameter of 2 nm. The heme active-site pocket is solvent accessible both from the inside and the outside of the ring. Moreover, a second anion binding site that could accommodate the assumed reaction intermediate ClO^- for further transformation has been identified near the active site.

The environment of the heme cofactor was investigated with electron paramagnetic resonance spectroscopy. Apart from the high-spin ferric signal of the five-coordinate resting-state enzyme, two low-spin signals were found corresponding to six-coordinate species. The current crystal structure confirms and complements a recently proposed catalytic mechanism that proceeds *via* a ferryl species and a ClO^- anion. Our structural data exclude cooperativity between the iron centers.

Keywords: heme-based oxygen production; chloro-oxyanions; remediation; *Azospira oryzae* strain GR-1; EPR

Introduction

Chlorite dismutase (Cld) catalyzes the reduction of the toxic compound ClO_2^- to environmentally innocuous Cl^- while producing O_2. This detoxification reaction is an essential step in the dissimilatory perchlorate reductive pathway. Recently, (per)chlorate-reducing bacteria have attracted attention due to their potential usefulness in remediation of water contaminated with oxyanions of chlorine. The toxic compounds perchlorate (ClO_4^-), chlorate (ClO_3^-), chlorite (ClO_2^-), and hypochlorite (ClO^-) are not formed on a large scale in nature. Although traces of perchlorate are found in Chile saltpeter, the use of such fertilizer has not been associated with the current contamination levels. The occurrence of harmful quantities of chloro-oxyanions in surface

*Corresponding author. E-mail address: d.de.geus@chem.leidenuniv.nl.

Abbreviations used: Cld, chlorite dismutase; MAD, multiple anomalous dispersion; MS, mass spectrometry; EPR, electron paramagnetic resonance.

and groundwaters in the United States is caused by the large-scale chemical production, the wide range of applications, and the chemical stability of chlorine anions in water. Most of the ClO_4^- contamination in the environment originates from the use of ammonium perchlorate as the solid oxidant in rocket propulsion, explosives, and fireworks.[1] ClO_3^- is used as a herbicide[2,3] and is released when chlorine dioxide (ClO_2) is used as a bleaching agent in the pulp and paper industry. ClO_2^- is a by-product of drinking water disinfection, with potential effects on the nervous system of children and a suspected health risk concerning anemia. The Environmental Protection Agency has therefore limited the maximum ClO_2^- concentration in drinking water to 1 mg/l†. *Azospira oryzae* strain GR-1 (DSM 11199) is one of the first described perchlorate-reducing bacteria.[4,5] This organism and its biochemical pathways that completely reduce ClO_4^- and ClO_3^- to Cl^- plus O_2 *via* the ClO_2^- intermediate have been subjects of research for more than a decade. This research was inspired by potential practical applications in waste water treatment and by fundamental interest in the mechanism of chlorite transformation. The key enzymes of the dissimilatory (per)chlorate-reducing pathway, (per)chlorate reductase and Cld, were originally purified and characterized from *A. oryzae* strain GR-1.[6,7] It was discovered that complete reduction of ClO_4^- by *A. oryzae* strain GR-1 into Cl^- and O_2 occurs in a few steps. First ClO_4^- is reduced to ClO_3^- by a (per)chlorate reductase (EC 1.97.1.1). Subsequently, the same enzyme catalyzes the reduction of ClO_3^- to ClO_2^-. Finally, Cld (EC 1.13.11.49) converts the ClO_2^- into Cl^- while producing O_2.

The (per)chlorate reductase contains one [3Fe–4S] cluster, two [4Fe–4S] clusters, and one molybdenum cofactor per $\alpha_3\beta_3$ heterodimer and produces a water molecule at each successive two-electron reduction step. Although many denitrifying bacteria can reduce ClO_3^- to ClO_2^- using nitrate reductase, the latter compound is toxic to these cells.[6]

Cld is a multimeric protein containing one iron protoheme IX per 28-kDa subunit.[7,8] Intriguing properties of this enzyme are the extraordinary specificity for chlorite and the efficiency of the chlorite conversion. Moreover, Cld is currently the only known heme-based enzyme that is able to perform O–O bond-formation catalysis as its primary function. An introduction to the current biochemical knowledge about Cld has been written by Streit and DuBois.[9] Recently, a mechanism involving a compound I intermediate and subsequent recombination of the resulting hypochlorite and compound I was proposed for the Cld reaction. In this study, high-valent oxo intermediates were characterized by stopped-flow UV–vis spectroscopy.[10] Here, we report the crystal structure of Cld, new insights into the quaternary state of the protein, and structural implications for the proposed catalytic mechanism.

† EPA 816-F-03-016 available for download at http://www.epa.gov/safewater/consumer/pdf/mcl.pdf.2003

Results and Discussion

Structure determination

The structure of Cld was determined by three-wavelength multiple anomalous dispersion (MAD) using the anomalous signal from iron atoms. The Cld crystallized in space group *P*21212, with unit cell dimensions of 164.46 Å×169.34 Å×60.79 Å. The crystals contained six molecules in the asymmetric

Table 1. Crystallographic data and refinement statistics

	Peak set	Inflection point	High-energy remote
A. *Data collection*			
Beam line	ESRF ID23-1	ESRF ID23-1	ESRF ID23-1
Wavelength (Å)	1.7382	1.7399	0.9834
Resolution range (Å)	50–2.7 (2.85–2.70)[a]	50–2.9 (3.86–2.90)	40.13–2.1 (2.21–2.10)
Reflections	660,269 (96,695)	538,131 (78,769)	731,403 (107,833)
Unique reflections	47,838 (6864)	38,886 (5579)	100,003 (14,403)
Multiplicity	13.8 (14.1)	13.8 (14.1)	7.3 (7.5)
Completeness (%)	100 (100)	100 (100)	100 (100)
Mean [I/SD(I)]	25.1 [6.3]	25.3 [6.1]	15.8 [3.8]
R_{sym} (%)[b]	10.7 (41.0)	10.9 (42.0)	10.5 (48.8)
R_{ano} (%)	3.8 (10.9)	3.4 (10.9)	4.3 (19.3)
Anomalous multiplicity	7.2 (7.2)	7.3 (7.3)	3.7 (3.7)
Anomalous completeness (%)	100 (100)	100 (100)	100 (100)
B. *Phasing*			
No. of Fe sites		6	
FOM overall		0.214	
FOM 2.21–2.10 Å		0.04	
C. *Refinement*			
Resolution range (Å)		40.13–2.10 (2.15–2.10)	
No. of reflections used in refinement		94,936 (6889)	
No. of reflections used for *R*-free		4994 (381)	
R-factor[c]		0.22 (0.25)	
R-free		0.25 (0.30)	
No. of protein/water atoms		10,939/555	
Average *B* value			
Protein/solvent (Å^2)		26.3/27.0	
Heme/HCO_3^-		20.9/42.2	
Thiocyanate		20.1	
Ramachandran statistics (%)[d]		94.7/5.3/0/0	
RMSD[e]			
Bonds (Å)		0.013	
Angles (°)		1.298	

[a] Values in parentheses are for the highest-resolution bin, where applicable. FOM, figure of merit.

[b] $R_{sym} = \sum_h \sum_i |I_{hi} - \langle I_h \rangle| / \sum_h \sum_i |I_{hi}|$, where I_{hi} is the intensity of the ith measurement of the same reflection and $\langle I_h \rangle$ is the mean observed intensity for that reflection.

[c] $R = \sum ||F_{obs}(hkl)| - |F_{calc}(hkl)|| / \sum |F_{obs}(hkl)|$.

[d] According to the program PROCHECK (Laskowski, R. A., MacArthur, M. W., Moss, D. S. & Thornton, J. M. (1993). PROCHECK: a program to check the stereochemical quality of protein structures. *J. Appl. Crystallogr.* **26**, 283–291). The percentages are indicated of residues in the most favoured, additionally allowed, generously allowed and disallowed regions of the Ramachandran plot, respectively.

[e] Estimates provided by the program REFMAC.[11]

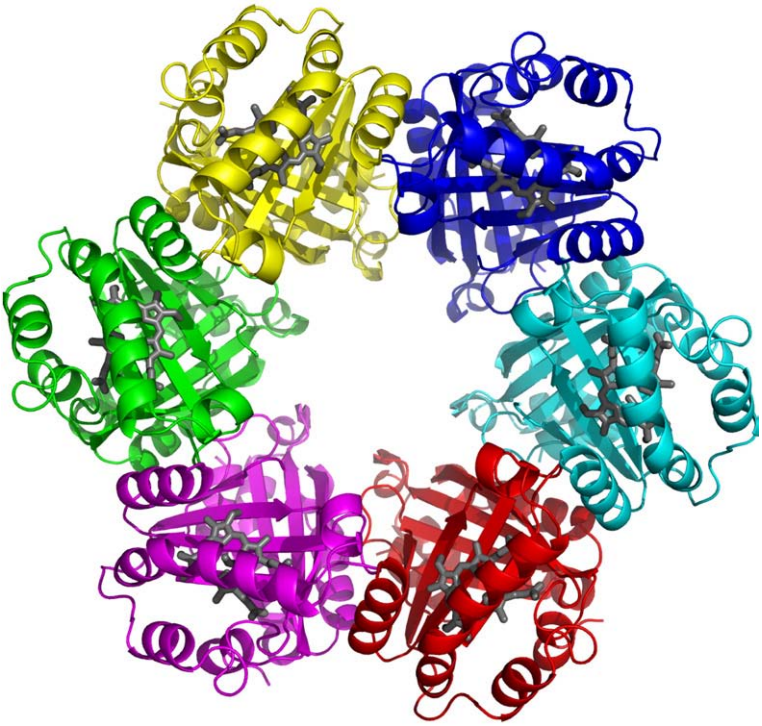

Fig. 1. Cld quaternary fold. View of the Cld quaternary fold. The six monomers are shown in different colors. The heme is depicted as sticks and shown in grey in all monomers.

unit, which results in a solvent content of 52.6% and a Wilson temperature factor of 26.6 Å^2. The electron density map for each monomer showed clear density of residues 8–217 and 231–248 (monomer A), 9–217 and 228–248 (monomer B), 10–217 and 229–248 (monomer C), 8–217 and 229–248 (monomer D), 8–217 and 229–248 (monomer E), and 9–217 and 231–248 (monomer F). All monomers contain one protoporphyrin IX (heme) and one thiocyanate in the active site. In all but one monomer (monomer

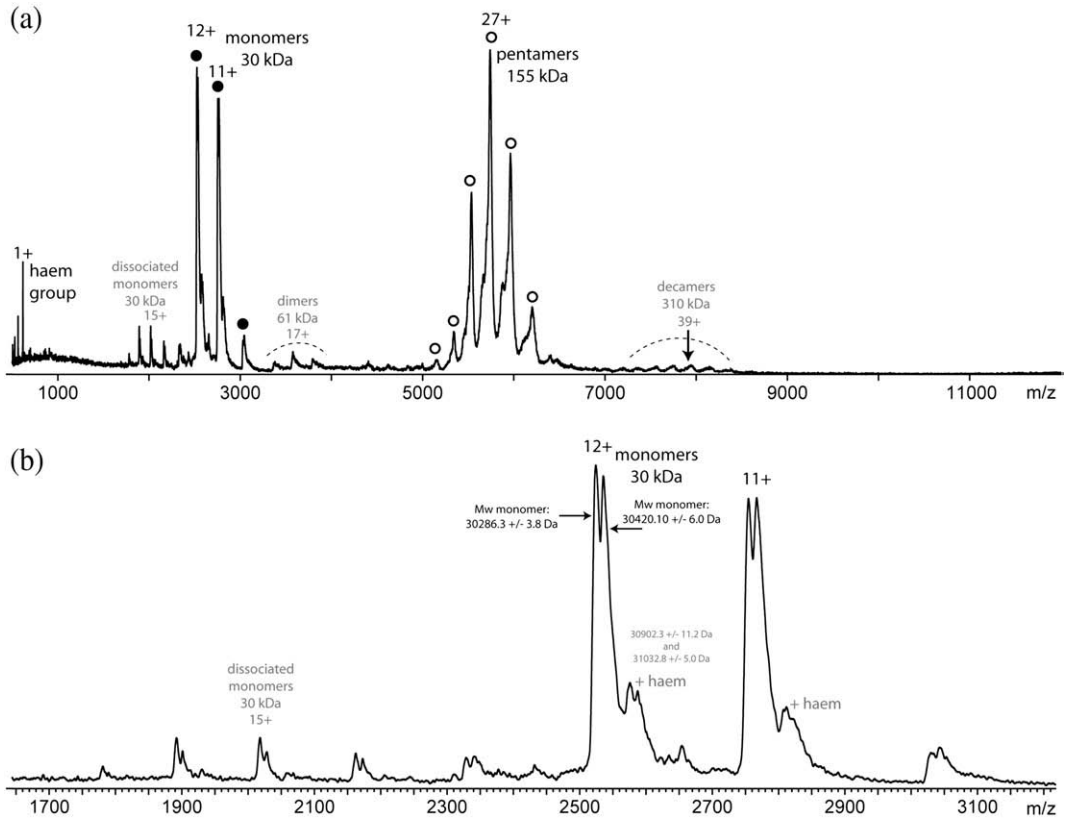

Fig. 2. Native MS of Cld. (a) Main mass spectrum of Cld electrosprayed from an aqueous ammonium acetate solution. (b) Close-up of the indicated region of the main spectrum showing the Cld monomeric mass.

D showed poor electron density), a hydrogen carbonate anion is present in close proximity to the heme. The final model has good stereochemistry and *R*-factors (Table 1) and contains 10,939 protein atoms, 6 heme molecules including 6 Fe^{3+}, 6 thiocyanate molecules, 5 hydrogen carbonate anions, and 555 water molecules.

Quaternary state of Cld

Cld forms a hexamer in the crystal. The six subunits form a 65 Å high ring with a maximum diameter of 90 Å. The inner diameter of the ring is approximately 20 Å (Fig. 1). A surface area of ~3000 $Å^2$ per monomer is buried, which is within

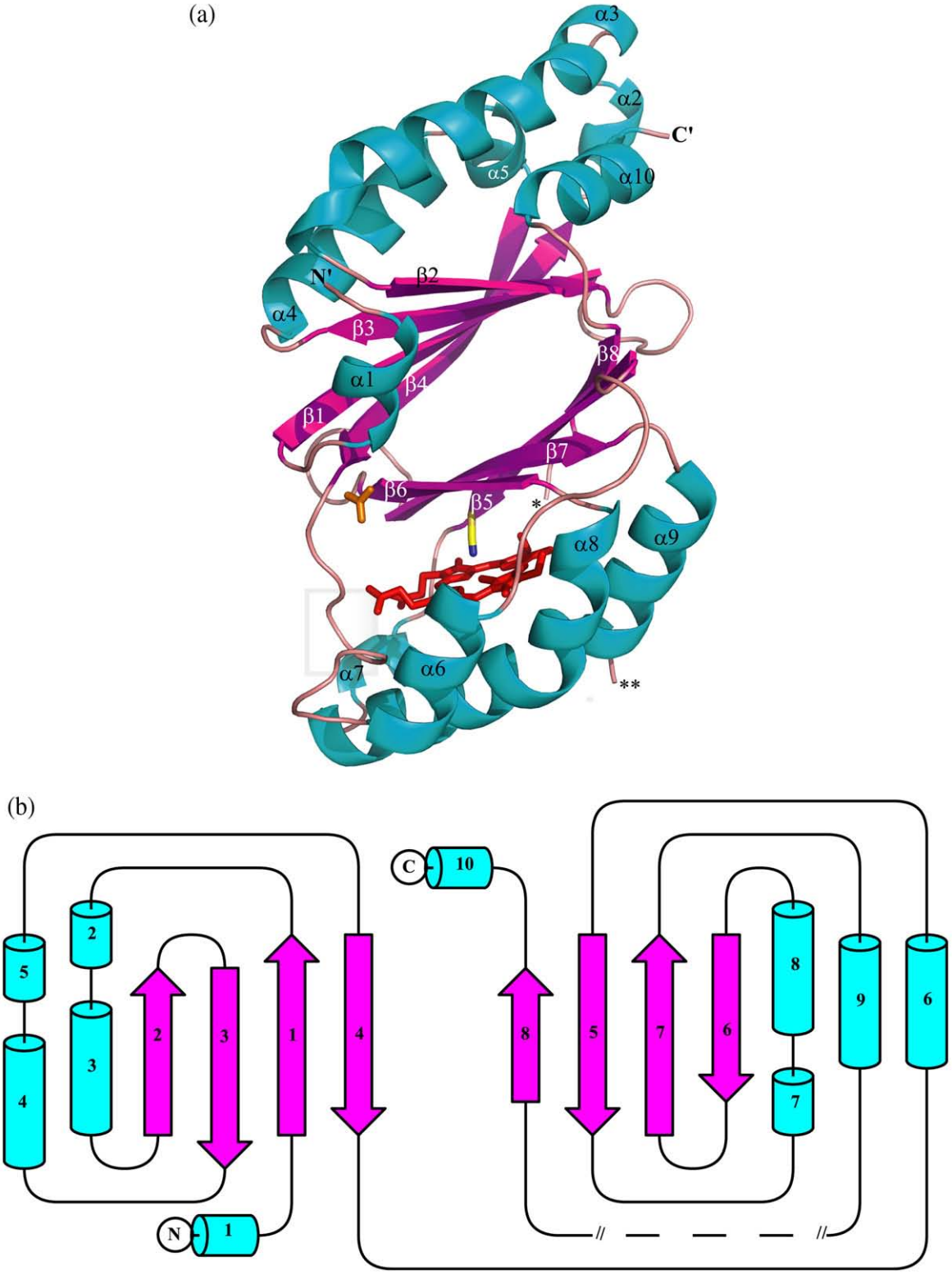

Fig. 3 (*legend on next page*)

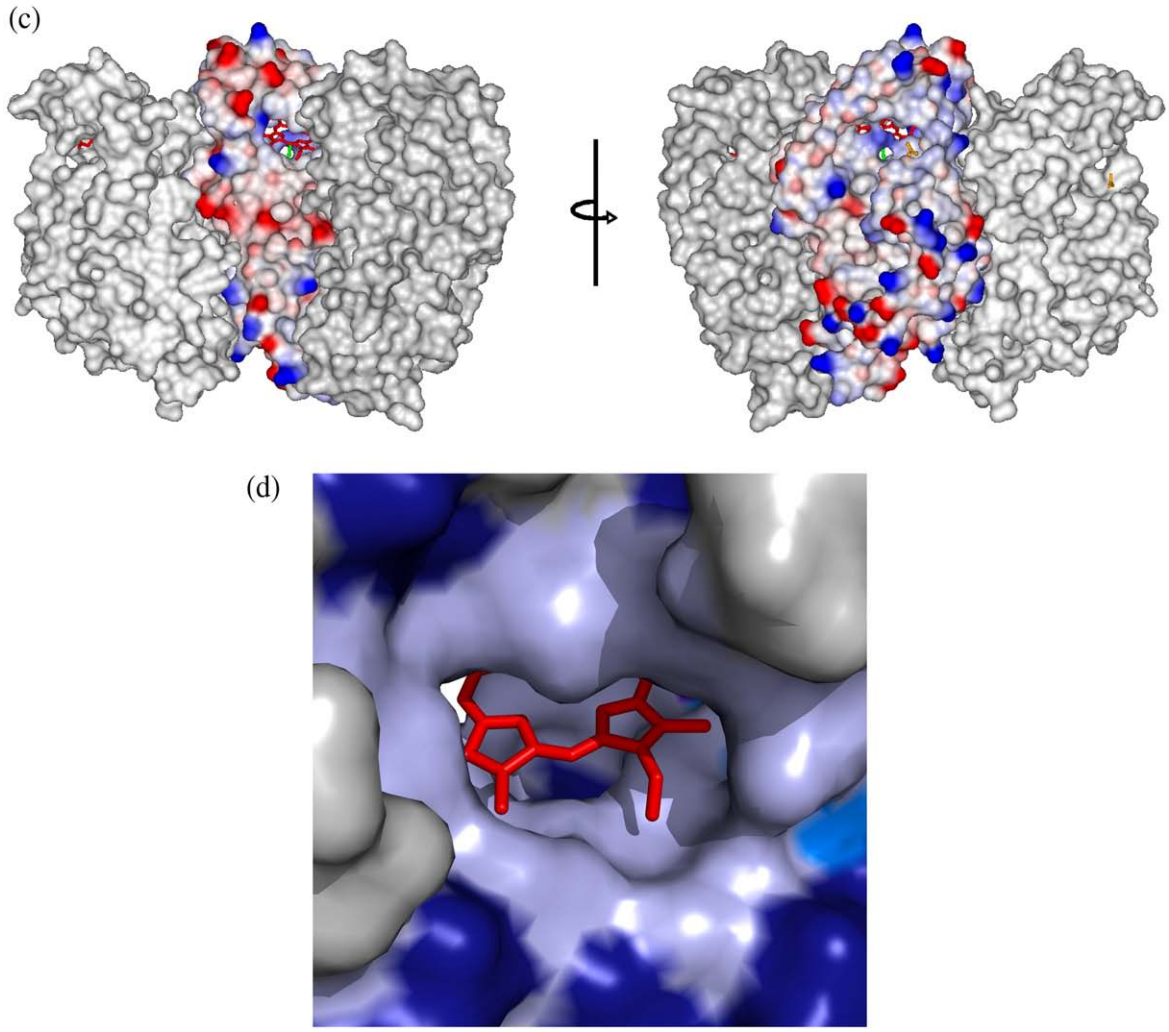

Fig. 3. Cld secondary structure and heme cavity. (a) View of the Cld overall fold. The α helices and β strands are labelled according to the ferredoxin fold and shown in light blue and purple, respectively. The heme is shown in red with the coordinating thiocyanate in yellow and blue (nitrogen atom). The amino acids forming the hydrogen-bond network (see also Fig. 2) are located within the boundaries of the grey frame. The hydrogen carbonate anion located next to β6 is shown in orange. In monomer A between **(Leu217) and *(Phe229), a part of the structure is not present due to a highly disordered loop. The picture was prepared with PyMol.[19] (b) Topology diagram of Cld. The α helices are depicted as light blue cylinders and the β strands as purple arrows. The 4↑1↓3↑2↓ and 8↑5↓7↑6↓ antiparallel β-sheet is a distinct feature. The topology diagram was prepared with TopDraw.[20] (c) Left: surface representation of three monomers viewed from the inside of the ring, perpendicular to the 6-fold noncrystallographic axis. Right: rotated 180° counterclockwise around the 6-fold noncrystallographic axis, showing the outside surface of the hexameric ring. The electrostatic surface of subunit A (negative and positive charges are indicated with red and blue, respectively) is represented amid the two flanking subunits E and F (grey surface). This figure shows the solvent accessibility of the heme cofactor (red) and the bound thiocyanate molecule (green). A hydrogen carbonate anion (orange) binds near the heme cavity at the end of a striking deep groove present on the outer surface of each monomer. (d) Surface representation of the Cld cavity. Increasing distances from the heme cofactor to amino acid residues are shown in different colors: up to 4 Å (light blue), 4–5 Å (marine blue), 5–6 Å (purple blue), and from 6–8 Å (dark blue). Residues farther away from the heme are depicted in grey. This shows the binding pocket underneath the heme available for accommodating the ClO_2^-.

the range of true oligomeric protein contacts rather than nonspecific crystal packing artefacts.[12] Previously, it was assumed that the wild-type and recombinant Cld from different sources formed tetramers.[7,9,13–15] These molecular weight determinations were based on analytical gel-filtration experiments that were calibrated with globular protein standards. However, the elution position of a protein on a gel-filtration column is not correlated with molecular weight, but instead is a function of the Stokes radius.[16] Using this relationship, we found that the Cld ring structure present in the crystal elutes at the same elution volume as a globular tetramer would (Fig. S1a and b).

To obtain a more accurate quaternary-state determination of Cld in solution, native mass spectrometry (MS) was performed. The mass spectrum

illustrates that the multimeric species of Cld in solution is preserved as a pentameric complex ion in the gas phase (Fig. 2a). The monomeric mass of Cld shows two peaks with a 134-Da difference, which was interpreted as a loss of the N-terminal methionine during expression (Fig. 2b). Using tandem MS, we confirmed the stoichiometry of the Cld oligomer to be a pentamer. By collisional activation of the ions, a single highly charged monomer was ejected from the pentamer. Concomitantly, low-charged tetramer counter complex ions were also observed.

It may be that the thiocyanate ion present in the crystallization condition affects the quaternary structure of Cld. Thiocyanate is a lipophilic ion that has the capacity to interfere with ionic pairs located either on the protein surface or in the hydrophobic core of folded proteins. Moreover, thiocyanate-dependent changes in quaternary state have been previously observed with flavoproteins.[17,18] Low concentrations of thiocyanate did not affect the quaternary state, as judged by mass spectrometry. Concentration levels of thiocyanate similar to that present in the mother liquor are too high for MS analysis.

Structure overview and the active site

The Cld monomer has an α+β structure consisting of an eight-stranded, antiparallel β-sheet forming a β-barrel with the α-helices lying next to these sheets on the outside of the protein (Fig. 3a). Each Cld monomer consists of two similar structural domains with a ferredoxin fold (Fig. 3b). A single ferredoxin fold contains a β-sheet formed by four antiparallel β-strands.[21] In a Cld monomer, the β-barrel is formed by the 4↑1↓3↑2↓ β-sheet from one domain and the topologically equivalent 8↑5↓7↑6↓ sheet from another (heme binding) domain. A heme (protoheme IX) is bound in a well-defined pocket between β-strands β5–β8 and α-helices α6–α9. This pocket is accessible from the inner channel as well as from the outside of the hexameric ring (Fig. 3c). The surface of the cavity is created by 31 conserved, mainly hydrophobic residues (boxed residues in Fig. 4). The iron atom in the heme cofactor is coordinated by His170 and (in our structure) a thiocyanate molecule. Thiocyanate was present in the mother liquor at a concentration of 0.3 M. Cyanide is a strong inhibitor (100%) at 20 mM concentration when the reaction was performed in the presence of 15 mM chlorite,[7] and we assume that thiocyanate is also an inhibitor of the reaction, indicating that the structure represents an inhibited state of the enzyme. Presumably, the thiocyanate will be replaced by chlorite in the reaction. To accommodate the substrate, a small distal cavity about 2 Å deeper (purple blue) than the surface of the surrounding heme cavity (light blue) is present (Fig. 3d). Two propionate groups of the heme cofactor (Fig. 5a) form hydrogen bonds with three water molecules and amino acids Asn117, Tyr118, Ile119, and Trp155. Residues 117–119 are present in the loop between β4 and α6 that connects the two ferredoxin-like domains. The Trp155 residue, present in α7, is conserved in all aligned sequences and resides in close proximity to the heme propionate side chain (Figs. 3a and 4). The corresponding Trp189 residue from *Dechloromonas aromatica* Cld has been suggested to generate the electron paramagnetic resonance (EPR)-active tryptophanyl radical appearing from a broad porphyrin π–cation radical signal in a Cld–chlorite mixture.[10] Strikingly, in cytochrome *c* peroxidase, a tryptophan residue is situated adjacent to the heme propionate, as in Cld. Moreover, based on kinetic data, Cld is predicted to share functional similarities with heme-dependent catalases and peroxidases.[9] Structural alignment of the active sites of cytochrome *c* peroxidase and Cld shows a conserved arginine (residue 183 in Cld) at a similar position in the distal heme pocket (Fig. 5b). The presence of a positively charged side chain can promote charge separation in the transition state. In cytochrome *c* peroxidase, the distal arginine has a key role in activating the substrate and its side chain shifts toward the active site in the presence of an anionic ligand.[27]

In Cld, Arg183 is present in a rather striking conformation, at a distance of 6.5 A from the iron atom. It seems to be displaced from the iron by the thiocyanate. Modelling indicates that in the absence of thiocyanate, the Arg183 can approach the iron atom to a distance of 2.8 Å without changing the positions of main-chain atoms. At a distance of 12 Å from the iron atom and 6.4 Å from Arg183, a hydrogen carbonate anion is located (Fig. 3c and Fig. S2), making a hydrogen bond (2.6 Å) with the backbone oxygen from Lys114. Inhibition studies

Fig. 4. Alignment of Cld homologues. Multiple sequence alignment of *A. oryzae* strain GR-1 Cld and related proteins using ClustalW[22] and GeneDoc.[23] The numbering is according to the residue numbers of AoCld in the PDB (entry 2vxh). The first six sequences are Clds from the different organisms: AoCld, *A. oryzae* strain GR-1; DspCld, *Dechlorosoma* sp. KJ; DaCld, *D. aromatica* RCB; PcCld, *Pseudomonas chloritidismutans*; IdCld, *Ideonella dechloratans*; DgCld, *Dechloromonas agitata*. Signal sequences were predicted with SignalP[24] and removed. BtDyp and SoTyrA are dye-decolorizing peroxidases from *Bacteroides thetaiotaomicron* and *Shewanella oneidensis*, respectively. Tt1485 is a hypothetical protein from *T. thermophilus* HB8 with remote homology to Cld, suggested to function as a novel heme peroxidase. BsT0T is a putative Cld from *B. stearothermophilus* with PDB entry 1t0t. PpMli is *Pseudomonas putida* muconolactone isomerase, a protein structurally similar to Tt1485. However, residues in the active sites of Tt1485 and PpMli are not conserved, implying that the proteins are not functionally related.[25] Residues conserved in the aligned sequences are shown white on black (100% identical), white on grey (70%), or black on grey (50%). The residues in AoCld directly involved in heme binding are marked with asterisks, while those forming the heme cavity are boxed. Note that Trp155 is a conserved residue in all sequences that partakes in formation of the heme pocket. The column labeled with ID% represents overall percentage sequence identity to AoCld.

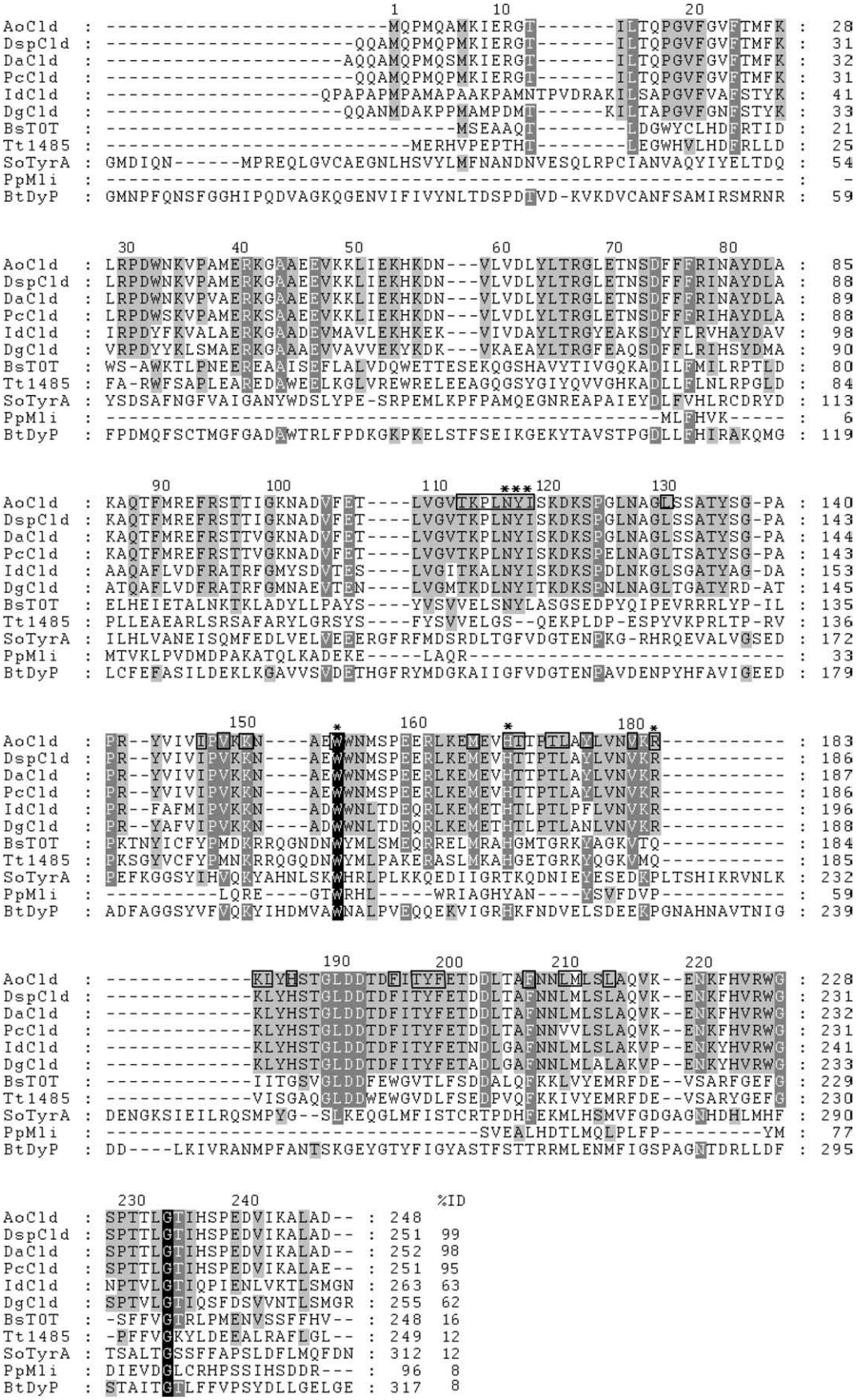

Fig. 4 (*legend on previous page*)

on Cld have suggested the presence of a second, non-Fe coordinating site for ion binding in proximity of the heme, which would be necessary to accommodate the ClO^- until further recombination with compound I.[9] The identification of the anion binding site in the Cld crystal structure, currently accommodating the hydrogen carbonate, points at a catalytic mechanism *via* ClO^- as proposed by Streit and DuBois[9] and, recently, experimentally supported by Lee *et al.*[10]

Comparison with other structures

The sequence alignment shows that Cld is a highly conserved protein in perchlorate respiring bacteria. This high level of similarity is also observed when the 31 residues of the heme-binding site of AoCld are compared with its homologues. Except for P115, Y177 (identities in four of six Cld sequences) and L211, M212 (identities in five of six Cld sequences) all these residues are completely conserved in the six Cld sequences shown (Fig. 4). No significant homology to any other enzyme could be found when BlastP was used on all nonredundant protein sequences in the National Center for Biotechnology Information database.[28] The highest percentage identity, excluding Cld homologues, was 23% with a ferrochelatase from *Propionibacterium acnes*. Ferrochelatase catalyzes the insertion of ferrous iron into protoporphyrin IX as the terminal step in heme biosynthesis. However, this protein has a three-layer αβα architecture with a chelatase-like fold [Protein Data Bank (PDB) code 1ak1] and did not show any similarity with AoCld by Superpose with secondary-structure matching.[26] Structural alignment of AoCld and proteins in the PDB with the

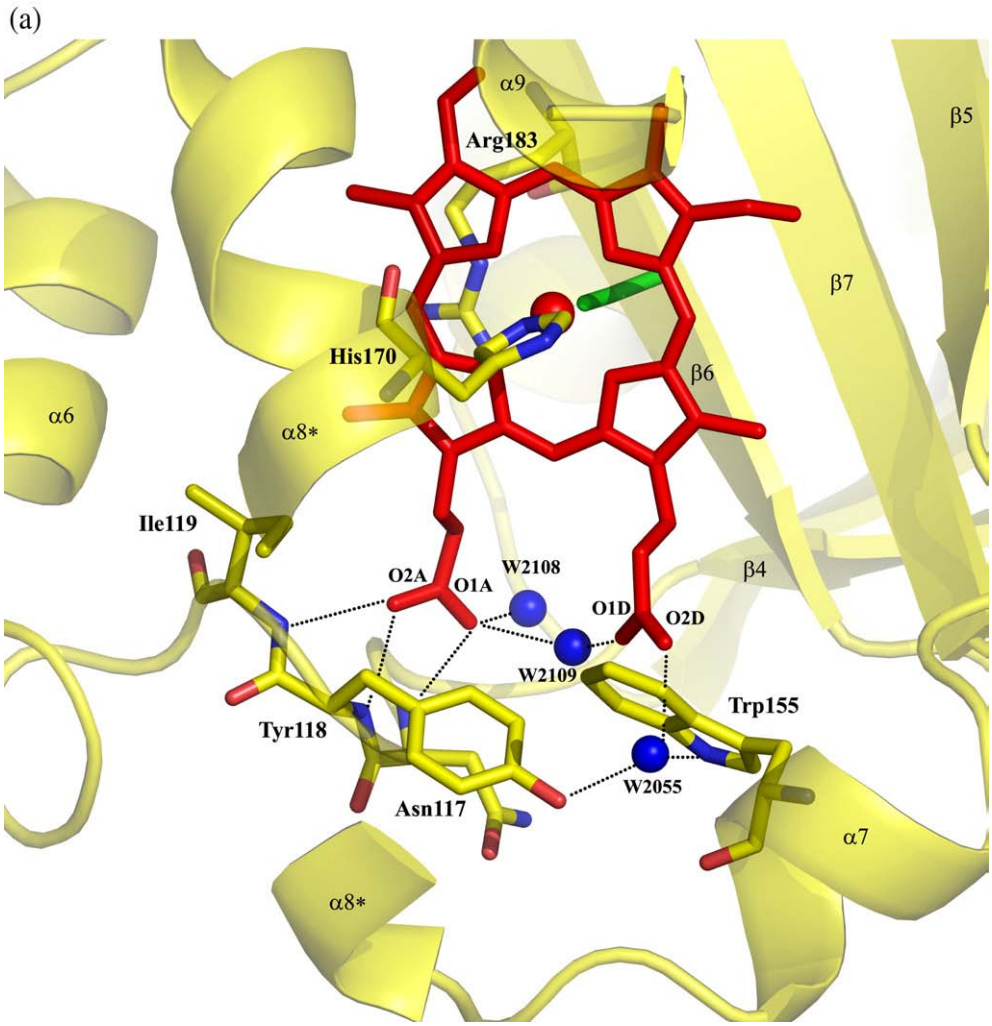

Fig. 5. Metal binding site and possible hydrogen bonds. (a) The heme is presented as red sticks, the coordinating His170 is yellow (carbon), blue (nitrogen), and red (oxygen). The same coloring is used for the amino acids Ile119, Tyr118, Asn117, Arg183, and Trp155. The coordinating thiocyanate is green and the water molecules (W) are depicted as blue circles. For clarity, a part of the helix α8 (between the asterisks) has been omitted from this drawing. The possible hydrogen bonds are presented as black dots. (b) Active-site superposition of cytochrome *c* peroxidase (PDB code 2cyp; labels and residues in grey) and Cld (2vxh; labels in black and residues in color) made with Superpose.[26] The proximal His, the distal Arg, and the Trp residues near the heme propionate group occupy comparable positions in the active sites of both enzymes.

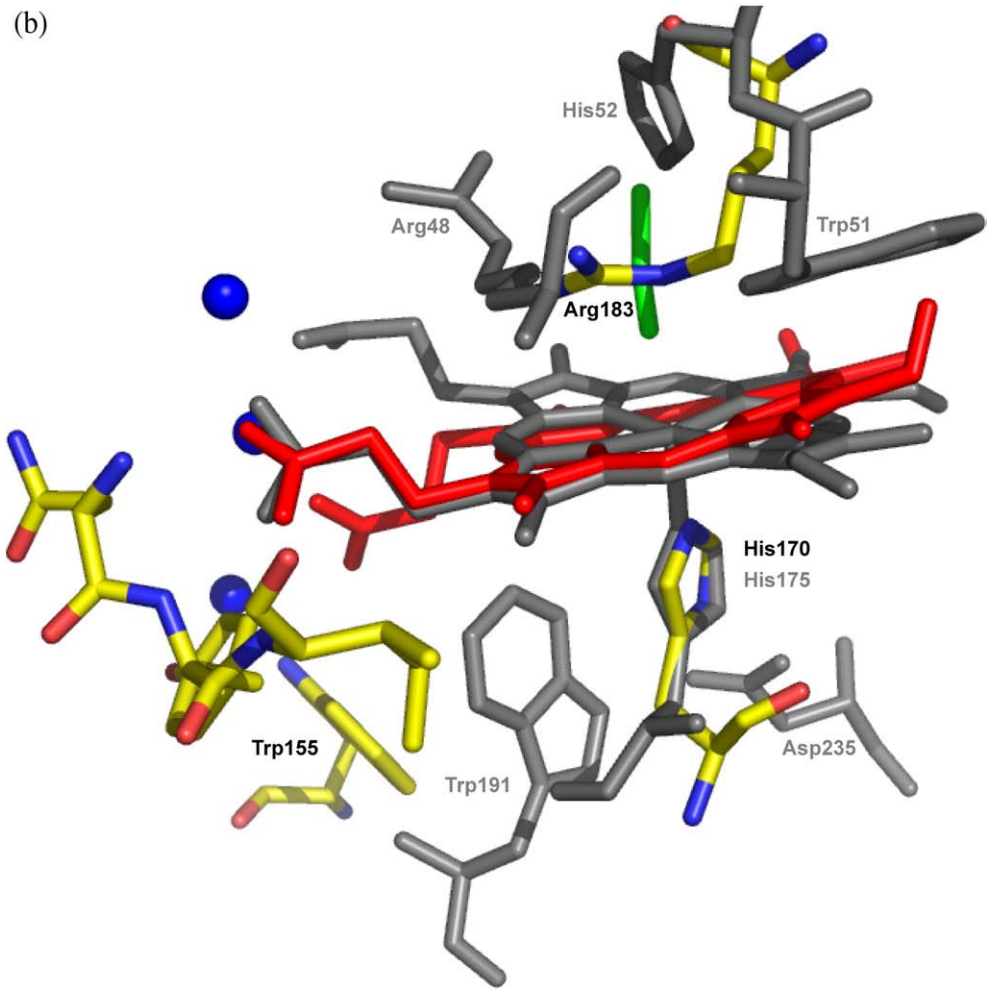

Fig. 5 (*legend on previous page*)

use of the Dali server[29] revealed the highest similarity with two proteins of unknown function (1t0t and 1vdh).[25] The sequence identities for 1t0t and 1vdx compared to Cld are 16% and 12%, respectively. Both proteins were superposed onto Cld using Superpose with secondary structure matching (Fig. 6). The main difference between the superposed structures is the orientation of the loop between β4 and α6, which is important for heme binding (Fig. 5). This loop contains three of the four residues able to form hydrogen bonds with the two propionate groups of the heme. The protein structures of 1t0t and 1vdh were elucidated by X-ray crystallography, and both had no heme present in the binding pocket. The putative Cld from *Bacillus stearothermophilus* with PDB entry 1t0t, present as a pentamer in the crystal, has not been described in the literature. The protein from *Thermus thermophilus* HB8 (1vdh) was described as a pentameric complex in the crystal structure, but reconstitution with heme did not result in significant Cld activity, indicating that 1vdh catalyzes a reaction other than with Cld.[25] Although the heme incorporating AoCld monomeric fold we report here is similar to crystal structures previously linked with Cld activity, the quaternary state is different.

Redox properties of recombinant Cld

An EPR-monitored redox titration of recombinant Cld showed the existence of three different heme species (Fig. 7a and b and Fig. S3). The first is a high-spin species with g values of 6.29, 5.46, and 1.99, similar to wild-type Cld[8] and *I. dechloratans* Cld,[30] which represents the five-coordinate ferric active form of the enzyme. The second is a low-spin species with g values of 2.97, 2.23, and 1.49, similar to wild-type Cld with imidazole bound at the sixth coordination site. This species is most likely a remnant of the His-tag purification procedure. And finally, at relatively high potentials another low-spin species is observed, with g values of 2.90, 2.26, and 1.55, which is indicative of a nitrogenous ligand at the sixth position. Presumably, this signal derives from a different protonation state of imidazole. In *I. dechloratans* Cld, a new low-spin ferric species was also found in the heterologously expressed enzyme, with g values of 3.04, 2.25, and 1.52. This species, which was not present in the

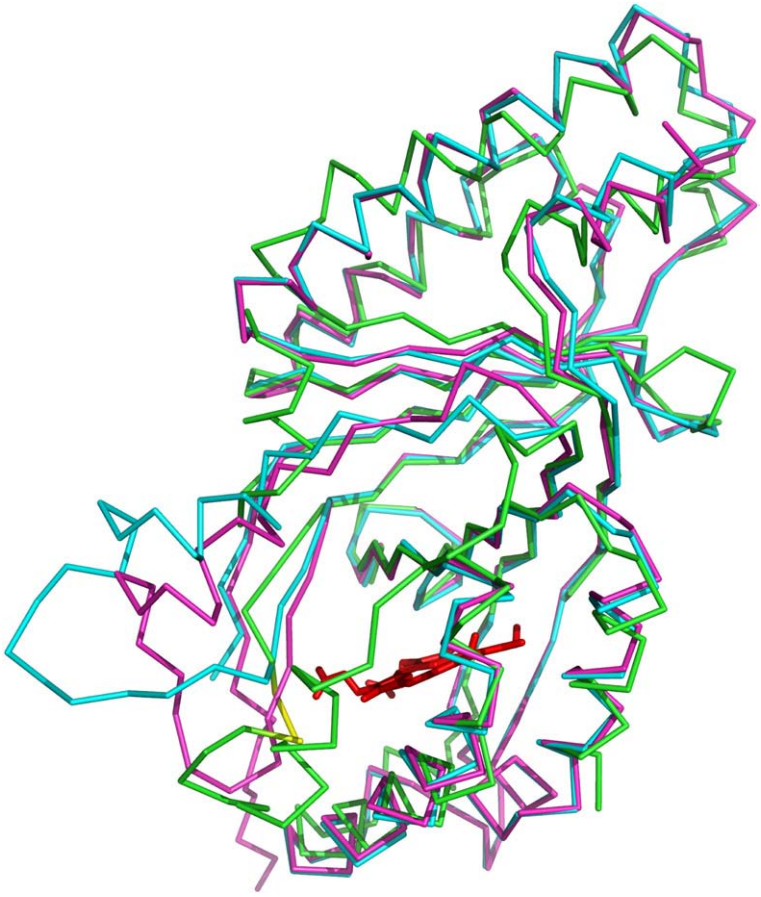

Fig. 6. Superposition of AoCld with two structural relatives. C^{α} superpositions of AoCld, a putative Cld from *B. stearothermophilus* (PDB code 1t0t) and a suggested heme peroxidase from *T. thermophilus* remotely homologous to Cld (1vdh showing that these enzymes share major structural features. Cld (2vxh) is shown in green, the putative Cld (1t0t) in blue, and the suggested heme peroxidase (1vdh) in magenta. The heme, present only in Cld (2vxh), is red. The main difference between the superposed structures is the orientation of the loop between β4 and α6 (labelling according to Fig. 3a), which is important for heme binding. The Cld residues Asn117, Tyr118, and Ile119 are shown in yellow. The superposition was done with Superpose[26] using secondary-structure matching and the picture was prepared with PyMOL.[19]

wild-type enzyme, was attributed to bis-histidine coordinated heme.[30]

Redox titration resulted in the following reduction potentials of the different heme species: −158± 9 mV for the five-coordinate Cld, −170±6 mV for imidazole-bound Cld, and +22±6 mV for the putative protonated imidazole-bound Cld. The reduction potential for the recombinant Cld is 135 mV lower than that for the wild-type enzyme,[8] which could be caused by subtle structural differences in the proximity of the heme. The reduction potential of heme iron in enzymes with a proximal histidine ligand is modulated by the basicity of the proximal histidine.[31] Furthermore, the wild-type enzyme, unlike the heterologously expressed enzyme, has been in contact with the highly oxidizing compounds (per)chlorate and chlorite during the cultivation of the organism. This has led to differences between native and recombinant versions of the same enzyme in some previous cases, notably also in *I. dechloratans* Cld.[30] The low reduction potential of recombinant Cld results in a stabilization of the ferric state, which could be expected to be beneficial to its catalytic properties. However, the specific activity of the heterologously expressed Cld is similar to that of the wild-type enzyme.[8]

By using the relationship between the reduction potentials of the ligand-bound and free enzyme, one can determine the ratio of the K_d values of the ferric and ferrous forms of the enzyme for that ligand.

$$K_{d,red} = 10^{-\left(E_{m,bound} - E_{m,free}\right) nF/2.303RT} k_{d,ox}$$

From the E_m of the putative protonated imidazole-bound form, we calculate that the K_d of this ligand for ferrous iron is 150 times lower than that for ferric iron. This indicates a clear preference of the protonated ligand for ferrous iron.

Cld catalytic mechanism

The stoichiometry of the Cld reaction is 1 mol Cl^- and 1 mol O_2 out of 1 mol ClO_2^-.[7] Isotope experiments excluded water as a substrate of Cld, indicating that atoms in the oxygen gas product originate entirely from the ClO_2^- substrate.[32]

The heme groups in two adjacent monomers are too far away from each other (Fe–Fe distance ~31 Å) to suggest electronic interactions between the Fe centers. Furthermore, recent kinetic experiments on recombinant Cld from *D. aromatica* RCB, which is 98% identical in amino acid sequence to AoCld, show exponential decay of the enzymatic activity with increasing ClO_2^- concentration.[9] Since cooperativity between the monomers in Cld would have led to a sigmoidal activity curve, this type of response to ClO_2^- binding could be ruled out. As a consequence, high valence states of the heme iron

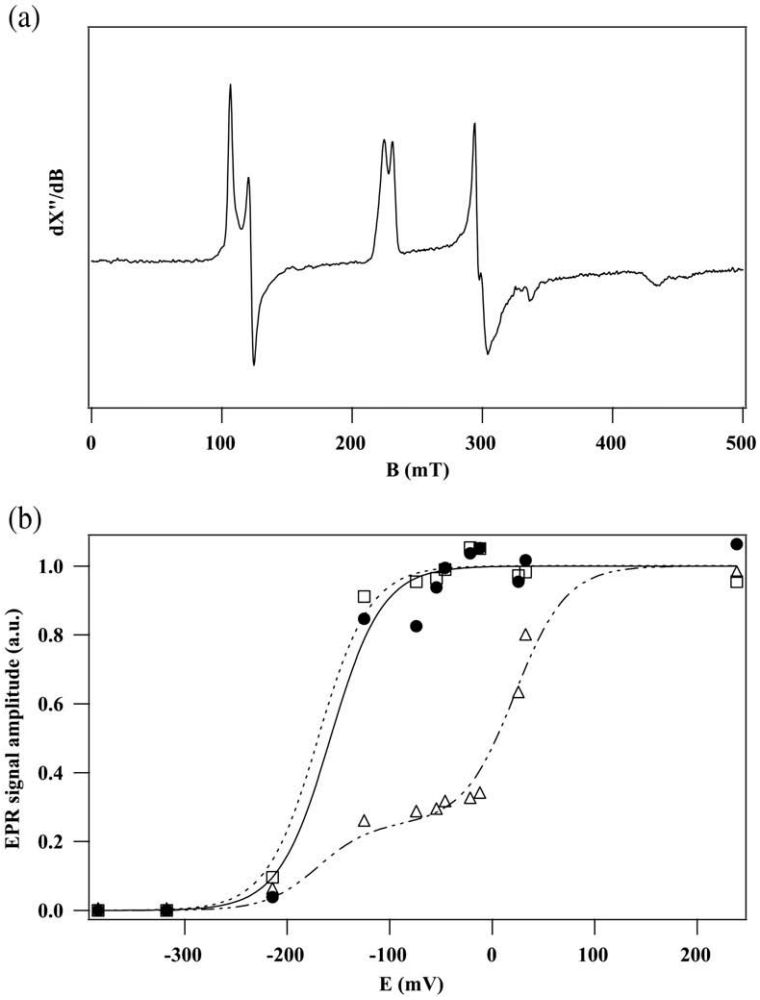

Fig. 7. EPR spectroscopy and redox titration of Ao Cld. (a) EPR spectrum of 0.18 mM Cld poised at +32 mV. EPR conditions: microwave frequency, 9.388 GHz; microwave power, 126 mW; modulation amplitude, 2.0 mT; temperature, 17.5 K. (b) Redox titration of Cld. (●) Five-coordinate heme, (□) imidazole adduct, (△) putative protonated imidazole-bound enzyme. The data points are fitted to the Nernst equation for a one-electron redox couple. Since the signal of the arginine-bound enzyme contains a contribution of the imidazole-bound enzyme, that signal is fitted to two independent one-electron redox couples.

seem to be crucial for the transfer of the total four electrons during one complete turnover, while the oxidation state of Cl in ClO_2^- changes from +3 to −1 in the Cl^- product.

Previous spectroscopic and ligand-binding studies of AoCld suggested binding of chlorite to the five-coordinate high-spin ferric form of the enzyme (or hexacoordinate with a weak sixth ligand) as the first step of the catalytic mechanism. The accessibility of the ferric iron centers was shown using the substrate analog nitrite that produced a low-spin species upon binding to the ferric form of Cld.[8] The current crystal structure confirms that all heme groups in the Cld molecule are solvent accessible, both from the outside and from the inside of the protein ring.

Hagedoorn *et al.* found optical and EPR spectroscopic evidence for the formation of a hydrogen peroxide Cld complex, which showed a decrease in the ferric signal and appearance of a radical signal in the EPR spectrum.[8] Based on these results and the necessity of high valence states of the heme cofactor, we assumed the oxidation of the ferric iron center to an intermediate oxoferryl complex (Fe^{IV}=O) like compound I or II.[33] George[34] discovered that ClO^- and ClO_2^- were able to form compounds I and II in the heme enzyme horseradish peroxidase. Recently, both compound I and a compound II-associated tryptophanyl radical signal have been observed using EPR on a freeze-quenched Cld sample containing its substrate chlorite.[10]

The positively charged guanidinium group at the distal heme site makes Arg183 an ideal candidate to align with and activate the ClO_2^- in the active site before oxidation. The ClO^- then released needs to be captured and stabilized by an amino acid nucleophile, presumably a nitrogen or oxygen atom. The backbone oxygen of the strictly conserved Lys114, which is part of the anion binding site, is positioned near the heme edge and might fulfill this function. A mode of recombining the oxygen atoms of compound I and ClO^- to give the reaction products has been proposed to occur *via* a peroxyhypochlorite intermediate. A nucleophilic attack of ClO^- on the electrophilic compound I oxygen could produce this intermediate species before recombination to molecular oxygen, Cl^-, and concomitant return to the ferric starting state of Cld.[10]

Conclusion

Cld is a heme-based enzyme that selectively and effectively detoxifies chlorite with concomitant O–O

bond formation. The removal of the by-product chlorite is essential for survival of perchlorate and chlorate respiring bacteria. Cld from different sources has been described as a tetramer in its native state. However, in our crystal, we observed a hexameric Cld ring. Based on the size of the solvent-accessible surface area buried after interaction between the six monomers, the hexamer was classified as a possible quaternary biological assembly. Reinterpreting our chromatographic data, we found that based on the experimentally determined elution position, Cld could also be a pentameric or a hexameric ring. Native MS using a multimeric sample with high enzymatic activity demonstrated the presence of a molecular weight corresponding to that of a Cld pentamer. Taking all these data together, we conclude that the pentamer is an active state of Cld in solution. We cannot exclude the hexamer to be another biologically relevant quaternary state, although it was impossible to measure its activity due to the presence of the thiocyanate inhibitor. However, since cooperativity between the Cld monomers has been excluded based on kinetics results, indicating the monomers independently catalyze chlorite reduction, the precise quaternary state of the enzyme may be less relevant for enzymatic activity. In this case, different quaternary states might be biologically relevant and enzymatically active. For example, there may be equilibrium between two states, with a transition influenced by protein concentration, pH, or a small molecule or an ion.[35,36]

The crystal structure of the inhibited, heme-incorporated Cld presented here gives the first insights into the active site of the O–O bond formation and points at some key residues. A strictly conserved histidine (His170) is the axial heme ligand, while a strictly conserved arginine residue (Arg183) occupies a similar position in the distal part of the active site as Arg48 in cytochrome *c* peroxidase. Arg183 most likely has an essential role in substrate positioning and activation as the homologous arginine residue in cytochrome *c* peroxidase. Trp155, another strictly conserved residue in Cld has been identified on geometrical grounds as the electron donor for the reduction of compound I to compound II. Trp155 is also part of the hydrogen-bond network that binds the heme cofactor.

The identification of an anion binding site near the heme is an important finding for the interpretation of the catalytic mechanism. The assumed mechanism involving a compound I intermediate would also generate a ClO^- anion that must remain close to the active site to perform its nucleophilic attack on the oxyiron species.

On the basis of the EPR-monitored redox titration, the reduction potential for the recombinant Cld heme appeared 135 mV lower than that for the wild-type enzyme. However, this does not result in a higher specific activity, as could be expected from the stabilization of the ferric state.

To conclude, our data support the proposed catalytic mechanism for O–O bond formation *via* high-valent oxyiron species and ClO^-. Furthermore, we have analyzed the active site of Cld and indicated some key residues for chlorite conversion. Our work demonstrates that a unique biological function, chlorite detoxification, has led to a unique heme enzyme.

A combination of site-directed mutagenesis with spectroscopic and structural approaches is now necessary to complement the current catalytic mechanism. Pre-steady-state kinetics experiments should be performed to study the formation of the Cld–ClO_2^- intermediates.

Experimental Procedures

Cloning, overexpression, and purification of Cld from *A. oryzae* strain GR-1

The Cld gene was chemically synthesized without the region coding for the signal sequence and then cloned into the pET28a vector, creating the vector pET28a-CDBC (BaseClear, the Netherlands). The resulting expressed protein from this plasmid includes a His-tag with a thrombin cleavage site, extending the amino terminus with 20 extra amino acids: MGSSHHHHHHSSGLVPRGSH. The protein used in the crystallization trials was digested with thrombin to remove this linker. Details about the cloning, overexpression, and purification of Cld have been described.[13] The specific activity of the purified Cld was $(1.5 \pm 0.5) \times 10^3$ μmol ClO_2^- min^{-1} mg^{-1}.

Determination of Stokes radius

The molecular Stokes radius of Cld was estimated by calibrated gel-filtration chromatography on an ÄKTAxpress protein purification system (GE Healthcare). A HiLoad 16/60 Superdex 200 prep-grade column equilibrated with 20 mM Tris–HCl (pH 7.5) and 135 mM NaCl was run at a low flow rate (0.3 ml min^{-1}). The column was calibrated using the following gel-filtration standards (Bio-Rad) with known molecular weights and radii: thyroglobulin (670 kDa, 86.0 Å), bovine gamma globulin (158 kDa, 52.3 Å), chicken ovalbumin (44 kDa, 30.5 Å), and equine myoglobin (17 kDa, 19.1 Å).[37,38] Samples were loaded onto the Superdex column and the relative elution volume $(-\log K_{av})^{1/2}$ was plotted *versus* the molecular Stokes radius. The partition coefficient, K_{av}, was calculated from the elution volume of the protein, V_e, and the total gel bed volume, V_t, using the expression $K_{av} = (V_e - V_0)/(V_t - V_0)$. The void volume, V_0, was determined by running blue dextran (average molecular mass, 2000 kDa) through the Superdex column.

Mass spectrometry

MS measurements were performed in positive ion mode using an electrospray ionization time-of-flight instrument (LCT, Waters, UK) equipped with a Z-spray nanoelectrospray ionization source. Needles were made from borosilicate glass capillaries (Kwik-Fil, World Precision Instruments, Sarasota, FL) on a P-97 puller (Sutter Instruments, Novato, CA), coated with a thin gold layer by using an Edwards Scancoat (Edwards Laboratories, Milpitas, CA) six Pirani 501 sputter coater.

Cld was buffer-exchanged to 50 mM ammonium acetate (pH 6.8) using centrifugal filter units with a cutoff of

30 kDa (Millipore, UK). Cld was analyzed at a monomer concentration of 5 μM. To produce intact gas-phase ions from large complexes in solution, the source was operated at a pressure of 6.7 mbar.[39] Mass spectra were recorded with a capillary voltage of 1.3 kV and cone voltage of 200 V. The ToF pressure was 1.2×10^{-6} mbar. Spectra were mass calibrated using an aqueous solution of CsI (25 mg/ml).

Tandem mass spectrometry

Tandem mass spectra were recorded on a modified Q-ToF 1 instrument (Waters) in positive ion mode. The pressure in the source region was increased to 10 mbar. Xenon was used as collision gas at a pressure of 1.5×10^{-2} mbar. The capillary voltage and cone voltages were kept at 1400 and 175 V, respectively. The collision voltage was varied from 10 to 200 V.

Activity assay with the Clark oxygen electrode

Cld activity was measured amperometrically by the evolution of O_2 using a modified Clark electrode (YSI) with home-made instrumentation, a Labview interface (National Instruments) and home-made Labview data acquisition and analysis software as described previously.[40] The assay was performed in 100 mM KP_i (pH 7.0) at 25 °C. After removal of oxygen by bubbling with high-purity argon, $NaClO_2$ was added to 6 mM final concentration. The reaction was started by adding 2–8 nM (final concentration) Cld.

EPR spectroscopy and redox titration

To determine the midpoint potential of the heme iron of Cld, an EPR-monitored redox titration was performed in an anaerobic glove box (Coy). The titration buffer was 50 mM KP_i (pH 7.2) with 10% glycerol. A mediator mix was prepared in the same buffer containing (per 100 ml) 2.6 mg N,N,N′,N′-tetramethyl-p-phenylendiamine, 5.2 mg dichlorophenol indophenol, 5.4 mg phenazine ethosulfate, 6 mg methylene blue, 3.8 mg resorufine, 7.5 mg indigodisulfonate, 2.8 mg 2-OH-1,4-naphtaquinone, 5.3 mg anthraquinone-2-sulfonate, 5.2 mg phenosafranin, 5.6 mg safranin O, 4.6 mg neutral red, 6.6 mg benzyl viologen, and 5 mg methyl viologen. To the titration vessel were added 0.32 ml 1.5 mM Cld, 1.0 ml mediator mix, and 1.28 ml titration buffer. The titration cell was connected to a reference Ag/AgCl electrode (SSE) and a platinum wire electrode. The electrodes were connected to a voltmeter. The potential was varied using sodium dithionite and potassium ferricyanide as reducing and oxidizing agent, respectively. At various potentials, 200-μl samples were taken from the titration vessel, transferred to an EPR tube, and immediately frozen in liquid nitrogen. EPR data were recorded on a Bruker ER200D EPR spectrometer with Labview interface (National Instruments) and home-made Labview data acquisition and analysis software; liquid helium cooling was as previously described.[41] The microwave frequency was measured with an HP5350B microwave frequency counter. The modulation frequency was always 100 kHz.

Crystallization

The crystallization of Cld has been published in detail elsewhere.[13] Briefly, after optimization trials, dark red cubic crystals up to approximately 100 μm × 100 μm × 100 μm in size were grown from well solutions containing 100 mM Mes buffer (pH 5.5), 25% (w/v) PEG MME (polyethylene glycol monomethyl ether) 2000, 0.3 M KSCN, 5% (v/v) glycerol, and 160–260 mM $(NH_4)_2SO_4$. Before data collection, the crystals were soaked in a solution containing the mother liquor including 16% glycerol.

Crystallographic data collection and processing

A MAD data set was collected on beam line ID23-1 at the European Synchrotron Radiation Facility (ESRF) at a wavelength of 1.7382 Å (peak), 1.7399 Å (inflection point), and 0.98340 Å (high-energy remote) using the anomalous signal of the iron atoms. The crystal was flash-frozen and kept at 100 K during data collection; 360 images were collected for the peak and inflection point and 185 images for the high energy, all with a rotation angle of 1°. Reflections were integrated with MOSFLM[42] and merged with SCALA[43] from the CCP4 suite.[44] For data statistics, see Table 1 and Ref. 13.

Structure solution and refinement

The structure was built automatically, with over 90% of the residues correctly docked, with the Crank[45] structure solution suite (version 1.2.0) using the three-wavelength MAD data. Crank used Scaleit[44] for scaling the data sets, Afro (Pannu, in preparation) for Fa estimation, Crunch2[46] for substructure determination, Bp3[47] for phasing, Solomon[48] for enantiomorph determination and density modification, and Buccaneer[49] with Refmac5[11] using the MLHL function[50] for automated model building and refinement.

Manual rebuilding of the model and addition of the unbuilt residues was done with COOT.[51] Refinement to 2.1 Å resolution was done with REFMAC including NCS restraints for residues 10–217 and 231–248; water molecules were added with COOT. Illustrations were prepared with PyMOL.[19]

Protein Data Bank accession numbers

Coordinates and structure factors have been deposited in the PDB (accession code 2vxh).

Acknowledgements

We thank Dr Ir Bert Jansen for data collection and Dr R.A.G. de Graaff for helpful discussions. We are grateful to Dr David Flot and other members of the EMBL–ESRF Joint Structural Biology Group for providing crystallographic data collection facilities and help therewith.

Supplementary Data

Supplementary data associated with this article can be found, in the online version, at doi:10.1016/j.jmb.2009.01.036

References

1. Urbansky, E. T. (2002). Perchlorate as an environmental contaminant. *Environ. Sci. Pollut. Res. Int.* **9**, 187–192.
2. Loomis, W. E., Bissey, R. & Smith, E. V. (1931). Chlorates as herbicides. *Science*, **74**, 485.
3. Smith, E. A. & Oehme, F. W. (1991). A review of selected herbicides and their toxicities. *Vet. Hum. Toxicol.* **33**, 596–608.
4. Rikken, G. B., Kroon, A. G. M. & vanGinkel, C. G. (1996). Transformation of (per)chlorate into chloride by a newly isolated bacterium: reduction and dismutation. *Appl. Microbiol. Biotechnol.* **45**, 420–426.
5. Wolterink, A., Kim, S., Muusse, M., Kim, I. S., Roholl, P. J., van Ginkel, C. G. *et al.* (2005). *Dechloromonas hortensis* sp. nov. and strain ASK-1, two novel (per) chlorate-reducing bacteria, and taxonomic description of strain GR-1. *Int. J. Syst. Evol. Microbiol.* **55**, 2063–2068.
6. Kengen, S. W., Rikken, G. B., Hagen, W. R., van Ginkel, C. G. & Stams, A. J. (1999). Purification and characterization of (per)chlorate reductase from the chlorate-respiring strain GR-1. *J. Bacteriol.* **181**, 6706–6711.
7. van Ginkel, C. G., Rikken, G. B., Kroon, A. G. & Kengen, S. W. (1996). Purification and characterization of chlorite dismutase: a novel oxygen-generating enzyme. *Arch. Microbiol.* **166**, 321–326.
8. Hagedoorn, P. L., De Geus, D. C. & Hagen, W. R. (2002). Spectroscopic characterization and ligand-binding properties of chlorite dismutase from the chlorate respiring bacterial strain GR-1. *Eur. J. Biochem.* **269**, 4905–4911.
9. Streit, B. R. & DuBois, J. L. (2008). Chemical and steady-state kinetic analyses of a heterologously expressed heme dependent chlorite dismutase. *Biochemistry*, **47**, 5271–5280.
10. Lee, A. Q., Streit, B. R., Zdilla, M. J., Abu-Omar, M. M. & DuBois, J. L. (2008). Mechanism of and exquisite selectivity for O–O bond formation by the heme-dependent chlorite dismutase. *Proc. Natl Acad. Sci. USA*, **105**, 15654–15659.
11. Murshudov, G. N., Vagin, A. A. & Dodson, E. J. (1997). Refinement of macromolecular structures by the maximum-likelihood method. *Acta Crystallogr., Sect. D: Biol. Crystallogr.* **53**, 240–255.
12. Henrick, K. & Thornton, J. M. (1998). PQS: a protein quaternary structure file server. *Trends Biochem. Sci.* **23**, 358–361.
13. De Geus, D. C., Thomassen, E. A., van der Feltz, C. L. & Abrahams, J. P. (2008). Cloning, expression, purification, crystallization and preliminary X-ray diffraction analysis ofthyn chlorite dismutase: a detoxifying enzyme producing molecular oxygen. *Acta Crystallogr., Sect. F: Struct. Biol. Cryst. Commun.* **64**, 730–732.
14. Stenklo, K., Thorell, H. D., Bergius, H., Aasa, R. & Nilsson, T. (2001). Chlorite dismutase from *Ideonella dechloratans*. *J. Biol. Inorg. Chem.* **6**, 601–607.
15. Bender, K. S., O'Connor, S. M., Chakraborty, R., Coates, J. D. & Achenbach, L. A. (2002). Sequencing and transcriptional analysis of the chlorite dismutase gene of *Dechloromonas agitata* and its use as a metabolic probe. *Appl. Environ. Microbiol.* **68**, 4820–4826.
16. Siegel, L. M. & Monty, K. J. (1966). Determination of molecular weights and frictional ratios of proteins in impure systems by use of gel filtration and density gradient centrifugation. Application to crude preparations of sulfite and hydroxylamine reductases. *Biochim. Biophys. Acta*, **112**, 346–362.
17. Caldinelli, L., Molla, G., Pilone, M. S. & Pollegioni, L. (2006). Tryptophan 243 affects interprotein contacts, cofactor binding and stability in D-amino acid oxidase from *Rhodotorula gracilis*. *FEBS J.* **273**, 504–512.
18. Pollegioni, L., Iametti, S., Fessas, D., Caldinelli, L., Piubelli, L., Barbiroli, A. *et al.* (2003). Contribution of the dimeric state to the thermal stability of the flavoprotein D-amino acid oxidase. *Protein Sci.* **12**, 1018–1029.
19. DeLano, W. L. (2002). *The PyMOL Molecular Graphics System.*; http://pymol.sourceforge.net/.
20. Bond, C. S. (2003). TopDraw: a sketchpad for protein structure topology cartoons. *Bioinformatics*, **19**, 311–312.
21. Zhang, C. & Kim, S. H. (2000). The anatomy of protein beta-sheet topology. *J. Mol. Biol.* **299**, 1075–1089.
22. Larkin, M. A., Blackshields, G., Brown, N. P., Chenna, R., McGettigan, P. A., McWilliam, H. *et al.* (2007). Clustal W and Clustal X version 2.0. *Bioinformatics*, **23**, 2947–2948.
23. Nicholas, K. B., Nicholas, H. B., Jr & Deerfield, D. W. I. (1997). GeneDoc: analysis and visualization of genetic variation. *EMBNEW NEWS*, **4**, 14.
24. Bendtsen, J. D., Nielsen, H., von Heijne, G. & Brunak, S. (2004). Improved prediction of signal peptides: SignalP 3.0. *J. Mol. Biol.* **340**, 783–795.
25. Ebihara, A., Okamoto, A., Kousumi, Y., Yamamoto, H., Masui, R., Ueyama, N. *et al.* (2005). Structure-based functional identification of a novel heme-binding protein from *Thermus thermophilus* HB8. *J. Struct. Funct. Genomics*, **6**, 21–32.
26. Krissinel, E. & Henrick, K. (2004). Secondary-structure matching (SSM), a new tool for fast protein structure alignment in three dimensions. *Acta Crystallogr., Sect. D: Biol. Crystallogr.* **60**, 2256–2268.
27. Finzel, B. C., Poulos, T. L. & Kraut, J. (1984). Crystal structure of yeast cytochrome *c* peroxidase refined at 1.7-Å resolution. *J. Biol. Chem.* **259**, 13027–13036.
28. Altschul, S. F., Madden, T. L., Schaffer, A. A., Zhang, J., Zhang, Z., Miller, W. & Lipman, D. J. (1997). Gapped BLAST and PSI-BLAST: a new generation of protein database search programs. *Nucleic Acids Res.* **25**, 3389–3402.
29. Holm, L. & Sander, C. (1996). Mapping the protein universe. *Science*, **273**, 595–603.
30. Danielsson, T. H., Beyer, N. H., Heegaard, N. H., Ohman, M. & Nilsson, T. (2004). Comparison of native and recombinant chlorite dismutase from *Ideonella dechloratans*. *Eur. J. Biochem.* **271**, 3539–3546.
31. Banci, L., Bertini, I., Turano, P., Tien, M. & Kirk, T. K. (1991). Proton NMR investigation into the basis for the relatively high redox potential of lignin peroxidase. *Proc. Natl Acad. Sci. USA*, **88**, 6956–6960.
32. Wolterink, A. F. W. M. (2004). *Characterization of (Per) chlorate-Reducing Bacteria*. Thesis, Wageningen University, Wageningen, the Netherlands.
33. Dolphin, D., Forman, A., Borg, D. C., Fajer, J. & Felton, R. H. (1971). Compounds I of catalase and horse radish peroxidase: pi–cation radicals. *Proc. Natl Acad. Sci. USA*, **68**, 614–618.
34. George, P. (1953). Intermediate compound formation with peroxidase and strong oxidizing agents. *J. Biol. Chem.* **201**, 413–426.
35. Cabezon, E., Butler, P. J., Runswick, M. J. & Walker, J. E. (2000). Modulation of the oligomerization state of the bovine F1-ATPase inhibitor protein, IF1, by pH. *J. Biol. Chem.* **275**, 25460–25464.
36. Cabezon, E., Butler, P. J., Runswick, M. J., Carbajo, R. J. & Walker, J. E. (2002). Homologous and heterologous inhibitory effects of ATPase inhibitor proteins on F-ATPases. *J. Biol. Chem.* **277**, 41334–41341.

37. Crawford, A. W. & Beckerle, M. C. (1991). Purification and characterization of zyxin, an 82,000-dalton component of adherens junctions. *J. Biol. Chem.* **266**, 5847–5853.
38. Alazard, R., Mourey, L., Ebel, C., Konarev, P. V., Petoukhov, M. V., Svergun, D. I. & Erard, M. (2007). Fine-tuning of intrinsic N-Oct-3 POU domain allostery by regulatory DNA targets. *Nucleic Acids Res.* **35**, 4420–4432.
39. Tahallah, N., Pinkse, M., Maier, C. S. & Heck, A. J. (2001). The effect of the source pressure on the abundance of ions of noncovalent protein assemblies in an electrospray ionization orthogonal time-of-flight instrument. *Rapid Commun. Mass Spectrom.* **15**, 596–601.
40. Pouvreau, L. A., Strampraad, M. J., Van Berloo, S., Kattenberg, J. H. & de Vries, S. (2008). NO, N_2O, and O_2 reaction kinetics: scope and limitations of the Clark electrode. *Methods Enzymol.* **436**, 97–112.
41. Pierik, A. J., Hagen, W. R., Dunham, W. R. & Sands, R. H. (1992). Multi-frequency EPR and high-resolution Mossbauer spectroscopy of a putative [6Fe–6S] prismane-cluster-containing protein from *Desulfovibrio vulgaris* (Hildenborough). Characterization of a supercluster and superspin model protein. *Eur. J. Biochem.* **206**, 705–719.
42. Leslie, A. G. (1999). Integration of macromolecular diffraction data. *Acta Crystallogr., Sect. D: Biol. Crystallogr.* **55**, 1696–1702.
43. Evans, P. (2006). Scaling and assessment of data quality. *Acta Crystallogr., Sect. D: Biol. Crystallogr.* **62**, 72–82.
44. Collaborative Computational Project Number 4. (1994). The CCP4 suite: programs for protein crystallography. *Acta Crystallogr., Sect. D: Biol. Crystallogr.* **50**, 760–763.
45. Ness, S. R., de Graaff, R. A., Abrahams, J. P. & Pannu, N. S. (2004). CRANK: new methods for automated macromolecular crystal structure solution. *Structure,* **12**, 1753–1761.
46. de Graaff, R. A., Hilge, M., van der Plas, J. L. & Abrahams, J. P. (2001). Matrix methods for solving protein substructures of chlorine and sulfur from anomalous data. *Acta Crystallogr., Sect. D: Biol. Crystallogr.* **57**, 1857–1862.
47. Pannu, N. S., McCoy, A. J. & Read, R. J. (2003). Application of the complex multivariate normal distribution to crystallographic methods with insights into multiple isomorphous replacement phasing. *Acta Crystallogr., Sect. D: Biol. Crystallogr.* **59**, 1801–1808.
48. Abrahams, J. P. & Leslie, A. G. (1996). Methods used in the structure determination of bovine mitochondrial F1 ATPase. *Acta Crystallogr., Sect. D: Biol. Crystallogr.* **52**, 30–42.
49. Cowtan, K. (2006). The Buccaneer software for automated model building. 1. Tracing protein chains. *Acta Crystallogr., Sect. D: Biol. Crystallogr.* **62**, 1002–1011.
50. Pannu, N. S., Murshudov, G. N., Dodson, E. J. & Read, R. J. (1998). Incorporation of prior phase information strengthens maximum-likelihood structure refinement. *Acta Crystallogr., Sect. D: Biol. Crystallogr.* **54**, 1285–1294.
51. Emsley, P. & Cowtan, K. (2004). Coot: model-building tools for molecular graphics. *Acta Crystallogr., Sect. D: Biol. Crystallogr.* **60**, 2126–2132.